Evaluation of porous cathodes for the electrochemical reduction of nitrates and nitrites in alkaline waste streams

K. JHA and J.W. WEIDNER*

Department of Chemical Engineering, University of South Carolina, Columbia, SC 29208, USA
*(*author for correspondence)*

Abstract

This paper describes the mathematical modelling and experimental work performed to evaluate porous cathodes for the electrochemical reduction of nitrates and nitrites in alkaline waste streams. A dynamic model of a batch process was developed that included a divided cell with a porous cathode, a cation-selective separator, a planar anode, and reservoirs for electrolyte recirculation and gas–liquid separation. Constant current experiments were done using a divided cell with nickel foam as the porous cathode. The experiments were performed with a catholyte feed of either 0.6 M $NaNO_2$ or 1.95 M $NaNO_3$, both supported by a 1.33 M NaOH solution, a current density of 0.25 A cm^{-2} and a solution temperature of 32 °C. The experimental results showed that the ammonia production reaction is the dominant cathodic reaction ($\sim$80% of the current). Estimates of the kinetic parameters were obtained using the experimental data and the model. The model was then used to simulate and study the performance of the porous electrode compared to the planar electrode for a range of operating currents. The results showed that at the optimum current density for a planar electrode of 0.25 A cm^{-2}, use of a porous cathode results in one-third the energy costs and time required to achieve 95% destruction of nitrate and nitrite compared to a planar cathode. At 0.40 A cm^{-2}, the energy and time required to achieve 95% destruction was an order-of-magnitude less for the porous electrode.

List of symbols

a	interfacial area per volume of porous cathode (cm^{-1})
A	superficial electrode area (cm^2)
$C_{i,b,a}$	bulk concentration of species i in the anolyte (mol cm^{-3})
$C_{i,s,a}$	concentration of species i at the anode surface (mol cm^{-3})
D_i	diffusion coefficient of species i (cm^2 s^{-1})
$\mathscr{F}$	Faraday's constant (96 487 C mol^{-1})
F_k	molar flow rate of the gaseous species in reaction k (mol s^{-1})
i	solution current density (A cm^{-2})
I_{cell}	cell current (A)
I_k	partial current of reaction k (A)
j_k	reaction current density of reaction k (A cm^{-2})
$j_{o,ref,k}$	exchange-current density of reaction k at reference conditions (A cm^{-2})
L	thickness of porous cathode (cm)
M_i	moles of species i (mol)
N_i	flux of species i (mol cm^{-2} s^{-1})
n_k	number of electrons taking part in reaction k
P	operating pressure (atm)
Q_g	volumetric flow rate of gas (cm^{-3} s^{-1})

Q_l	volumetric flow rate of liquid (cm^{-3} s^{-1})
$\mathscr{R}$	Universal gas constant (8.314 J mol^{-1} K^{-1})
s_{ik}	stoichiometric coefficient of species i in reaction k
S_a	anode gap (cm)
S_c	cathode gap (cm)
S_s	separator thickness (cm)
T	temperature (K)
u	mean electrolyte velocity (cm s^{-1})
y	distance within the diffusion layer (cm)
y_i	mole fraction of species i in the gas phase
z	distance into the porous cathode (cm)

Greek letters

α_k	transfer coefficient in reaction k
δ_i	diffusion-layer thickness for species i (cm)
λ_w	electroosmotic drag coefficient of water
θ	volume of pores per unit volume of porous cathode (i.e., porosity)
θ_g	volume occupied by gas per unit volume of porous cathode
κ_c	effective conductivity of catholyte (Ω^{-1} cm^{-1})
κ_c°	conductivity of the bubble-free catholyte (Ω^{-1} cm^{-1})
ϕ_c	solution potential in the porous cathode (V)

1. Introduction

The Savannah River Site (SRS) in Aiken, SC, is a United States Department of Energy (DOE) facility where nuclear materials have been produced for defense and space programs. High level nuclear waste has been stored in underground carbon steel tanks since the startup of SRS in the 1950s. Figure 1 shows the process flowsheet for the proposed facility that will process the waste for permanent disposal. The process consists of the in-tank precipitation facility (ITP), an electrochemical reactor, off-gas processing and evaporator/crystallizer units. The ITP removes greater than 99.5% of radioactivity from the wastes, and the resulting high-level waste stream is immobilized in a borosilicate glass wasteform. The remaining low-level radioactive waste contains many hazardous substances, among which nitrates and nitrites are present in the highest concentration. Significant savings in waste disposal costs may be possible by destroying the nitrates and nitrites prior to disposal as a low-level saltstone.

Previous experimental work has shown the electrochemical reduction to be an effective treatment of nitrate and nitrite waste solutions [1–6]. For example, Hobbs and Ebra [1] electrolytically reduced nitrate and nitrite in both an undivided and a divided cell with a planar nickel cathode and a feed solution simulating that produced at SRS. High destruction ($\sim$99%) of nitrates and nitrites were obtained in a batch process with the products being ammonia, nitrogen, oxygen and sodium hydroxide. However, the per pass conversion was small [2] due to slow kinetics of the nitrate and nitrite reduction compared to hydrogen evolution. Li et al. [3] found that electrolysis of $NaNO_3$ in 3 M $NaOH$ and 0.25 M Na_2CO_3 at 80 °C using platinized nickel planar electrodes improved the efficiency of the reduction process with ammonia and nitrogen being the main products. The disadvantage of this process is the cost of the platinized electrodes. Here we use a mathematical model coupled with experimental data to evaluate porous nickel electrodes to determine the extent to which efficiency is improved compared to planar electrodes.

Mathematical models of a parallel-plate electrochemical reactor for nitrate and nitrite destruction have been developed previously [6–9]. The work by Prasad et al. [8] is of particular importance to the present work since they used a conventional boundary-layer approximation to incorporate the effects for diffusion and migration. The work by Prasad et al. [8] also contained some bench-scale experimental data that verified qualitative trends seen in the simulations, and the work by Wingard [9] reported more extensive data. In this paper, we follow the experimental procedure developed by Wingard [9], and we incorporate the boundary-layer approach used by Prasad et al. [8]. The performance of a porous cathode compared to that of a planar cathode for the reduction of nitrate and nitrite in alkaline waste streams will be evaluated by performing the following four tasks: (i) develop a model of a divided cell with a flow-through porous cathode, a cation-selective separator, and a planar anode; (ii) incorporate the divided cell model with porous and planar cathodes into the previously developed batch process model [8]; (iii) collect data on the experimental batch process containing a porous nickel cathode for use in the extraction of kinetic parameters; and (iv) use the model with the extracted parameters to compare the performance of a batch process with a porous cathode to that with a planar cathode.

2. Model development

The electrochemical reactor in Figure 1 is used to reduce the nitrates and nitrites to nitrogen, ammonia and nitrous oxide. The electrochemical reactor is a batch recirculation process shown in Figure 2. The main reactions occurring at the cathode are given below [7, 8]:
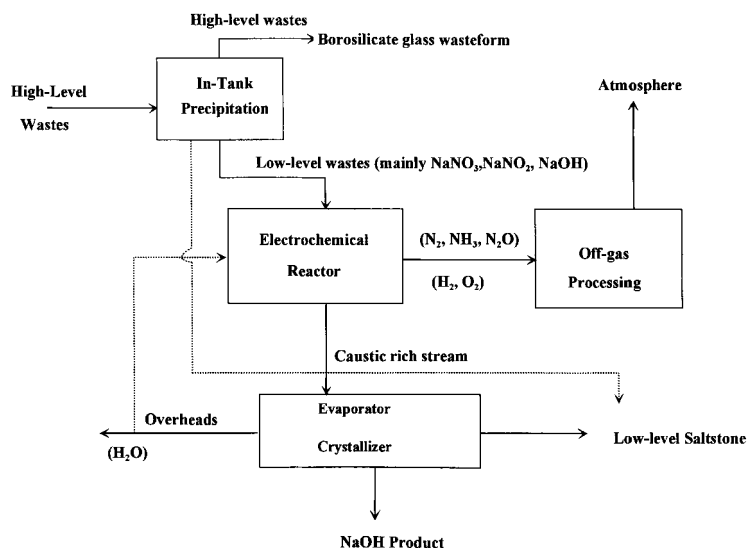

Fig. 1. Process flowsheet of the electrochemical treatment of liquid radioactive wastes.
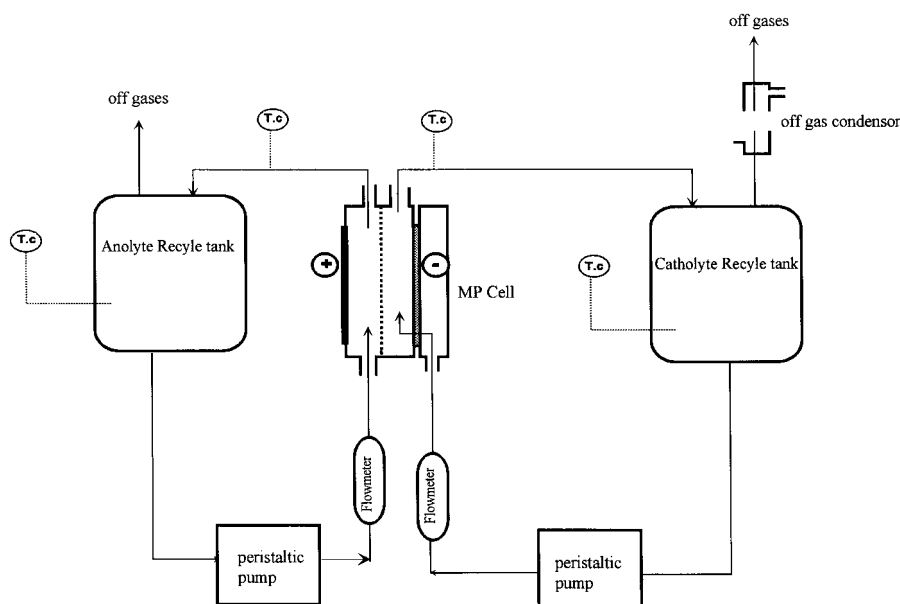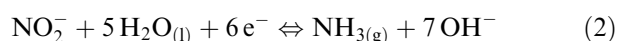
Fig. 2. Schematic of batch process with a porous cathode. Arrangement with a planar cathode is identical except that extra flow channel on the cathode side is not present.

$$NO_3^- + H_2O_{(l)} + 2\,e^- \Leftrightarrow NO_2^- + 2\,OH^- \quad (1)$$
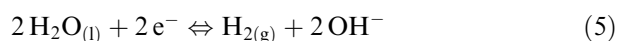
$$(U^\theta = 0.01\,\text{V vs SHE})$$

$$NO_2^- + 5\,H_2O_{(l)} + 6\,e^- \Leftrightarrow NH_{3(g)} + 7\,OH^- \quad (2)$$

$$(U^\theta = -0.165\,\text{V vs SHE})$$

$$2\,NO_2^- + 4\,H_2O_{(l)} + 6\,e^- \Leftrightarrow N_{2(g)} + 8\,OH^- \quad (3)$$

$$(U^\theta = 0.406\,\text{V vs SHE})$$

$$2\,NO_2^- + 3\,H_2O_{(l)} + 4\,e^- \Leftrightarrow N_2O_{(g)} + 6\,OH^- \quad (4)$$

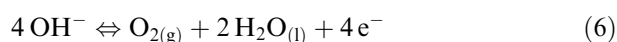$$(U^\theta = 0.15\,\text{V vs SHE})$$

$$2\,H_2O_{(l)} + 2\,e^- \Leftrightarrow H_{2(g)} + 2\,OH^- \quad (5)$$

$$(U^\theta = -0.828\,\text{V vs SHE})$$

In a divided cell with a cation-selective separator, the oxidation of nitrate to nitrite via Reaction 1, and the resulting inefficiency, is negligible. Therefore, the evolution of oxygen is the dominant reaction at the anode and is given by

$$4\,OH^- \Leftrightarrow O_{2(g)} + 2\,H_2O_{(l)} + 4\,e^- \quad (6)$$

$$(U^\theta = 0.401\,\text{V vs SHE})$$

Prasad et al. [8] developed a model of the batch process consisting of a planar cathode, a nonselective separator, a planar anode, and recirculation tanks. They used a boundary-layer assumption to account for the mass-transfer resistance of reactants to the surface of the cathode. A similar approach will be used here to account for mass-transfer resistance within the porous cathode and at the planar anode. A schematic of the divided cell is shown in Figure 3. Most of the model development is similar to the work by Prasad et al. [8], and therefore only assumptions and equations unique to this work will be shown here.

2.1. *Assumptions*

Below are a list of assumptions related to the porous cathode, and assumptions of the batch process that are different from those listed earlier [8]:

(i) The cation-selective separator allows only the sodium ions and water molecules to pass through from the anolyte to the catholyte.

(ii) The initial concentration of nitrogen, hydrogen, and nitrous oxide are at saturation values and any of these species produced from the Reactions 3–5
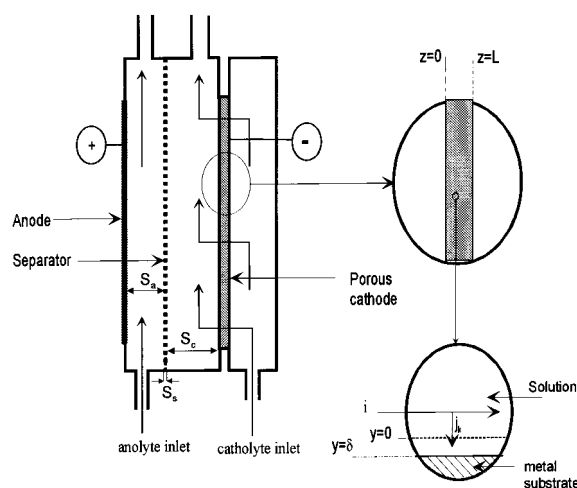

Fig. 3. Schematic of the divided cell with a porous cathode.

at the cathode and Reaction 6 at the anode are gaseous products.

(iii) The conductivity of the electrolyte is constant inside the diffusion layer in the cathode, while it can vary in the diffusion layer at the anode.

(iv) All the bulk concentrations, and hence the conductivity, in the anolyte remain constant with time and in the flow direction.

(v) All the bulk concentrations, and hence the conductivity, in the catholyte are uniform in the flow direction but change with time.

(vi) The moles of chloride and bromide added to the catholyte to track the water content of the catholyte do not change with time.

(vii) In the porous cathode, the matrix phase has constant porosity (θ), tortuosity (τ) and interfacial area per volume (a). It also has a very high electronic conductivity compared to that of the electrolyte, such that the potential within the metal matrix is uniform.

(viii) The thickness of the diffusion layer formed inside the pores of the cathode is constant throughout the electrode and is not affected by the generation of gas bubbles.

Assumption (ii) is valid as the solubility of hydrogen, nitrogen and nitrous oxide is small and therefore, saturation is achieved quickly. Assumption (iii) is valid since the catholyte is well supported while the anolyte is a binary electrolyte. The anolyte's bulk properties, including its conductivity, are assumed to be constant as the NaOH is constantly replenished during the batch process (assumption (iv)). Uniform concentration in the flow direction in assumptions (iv) and (v) is valid due to low single-pass conversion. Assumption (vi) was verified through analysis of the anolyte, which found no chloride or bromide present in this stream. Assumption (vii) is valid due to an inert porous cathode. Assumption (viii) was used previously to predict the reaction distribution for zinc deposition in a porous electrode [10]. Experimentally obtained reaction distributions were shown to agree well with model predictions at the high flow rates, and therefore low gas fractions, used in this study.

2.2. Porous cathode

Figure 3 shows a magnified view of the porous electrode region. According to porous-electrode theory [11], the ionic current, i, is related to the reaction currents, j_k, by

$$\frac{\mathrm{d}i}{\mathrm{d}z} = a \sum_{k=1}^{5} j_k \tag{7}$$

The reaction currents are related to the surface concentration of reactants and the solution potential by kinetic expressions given previously [8].

Prasad et al. [8] also derived expressions that relate the concentration of reactants at the electrode surface to bulk values using a boundary-layer approximation. This boundary-layer approach incorporates both the migra-tional and diffusional contributions to mass transfer. The only modification needed here is the empirical correlation used to estimate the boundary-layer thickness. The correlation applicable for the grade of nickel foam used in the present study is given as [12]:

$$\delta_i = \frac{4.5\,D_i a}{u^{0.30}} \tag{8}$$

Ohm's law relates the ionic current density to the solution potential by

$$i = -\kappa \frac{\mathrm{d}\phi_\mathrm{c}}{\mathrm{d}z} \tag{9}$$

where the Bruggeman equation [13] relates the conductivity of the electrolyte, κ_c, to its bubble-free conductivity, κ_c°, by:

$$\kappa_\mathrm{c} = \kappa_\mathrm{c}^\circ (\theta - \theta_\mathrm{g})^{1.5} \tag{10}$$

An empirical correlation is used to relate κ_c° to the concentrations of nitrate, nitrite and hydroxide ions [9]. The gradient of the gas porosity is related to the gas producing reaction currents as (see Appendix for derivation):

$$\frac{\mathrm{d}\theta_\mathrm{g}}{\mathrm{d}z} = a \left(\frac{\mathscr{R}TA(\theta - \theta_\mathrm{g})^2}{P\mathscr{F}\theta Q_1} \right) \sum_{k=2}^{5} \frac{j_k}{n_k} \tag{11}$$

The ammonia reaction current (j_2) only contributes to the gas fraction once the ammonia concentration reaches its saturation limit. In the short-term experiments performed here, the ammonia saturation limit is not reached.

The partial current for each reaction is related to the local reaction current by the following integral:

$$I_k = aA \int_0^L j_k \,\mathrm{d}z \tag{12}$$

2.3. Separator

The separator used in our studies was Nafion® 350, which is a cation-selective membrane. Among the ionic species present in the anolyte and catholyte, the separator allows only the sodium ions to pass through it. Besides sodium, water is also transported across the membrane due to electroosmotic drag. Therefore, the transport of only sodium and water across the separator needs to be considered. Faraday's law gives the flux of sodium through the separator as follows:

$$N_{\mathrm{Na}^+} = \frac{I_{\mathrm{cell}}}{A\mathscr{F}} \tag{13}$$

and the flux of water can be expressed as

$$N_{H_2O} = \lambda_w N_{Na^+} \qquad (14)$$

where λ_w is the net number of moles of water transported per mole of sodium. Experimental measurements [9] have determined that the λ_w is approximately 10 for Nafion® 350 in this system.

2.4. *Planar anode*

Although a planar anode was used by Prasad et al. [8], their nonselectrive membrane allowed both cations and anions to pass. For the cation-selective membrane used here, the anolyte remains a binary electrolyte at all times (i.e., OH^- and Na^+). Therefore, the concentration of the OH^- at the anode surface, $C_{OH^-,s,a}$, is related to its bulk value by

$$C_{OH^-,s,a} = C_{OH^-,b,a} - \frac{j_6 \delta_{OH^-}}{2\mathscr{F} D_{OH^-}} \qquad (15)$$

Note that j_6 is equal to I_{cell}/A since the anode is planar and oxygen evolution is the only reaction occurring at this electrode. The diffusion-layer thickness for the hydroxide is calculated using the correlations used earlier by Prasad et al. [8].

2.5. *Solution procedure*

The governing equations for the electrochemical cell and the recirculation tanks were programmed and solved using Speedup™ Aspen Technology's equation-based dynamic flowsheet simulator software. Speedup was used for two main advantages: (i) a choice of built-in time integrators and algebraic equation solvers; and (ii) the facility of linking the various reactor section models among each other and to models of other process units. The differential equations governing the porous cathode were discretized using three-point finite difference and Simpson's rule [14] was used to obtain the integral in Equation 13. Fourth order Runge–Kutta method was used to perform the integration in time. An absolute tolerance of 10^{-10} was used as the convergence criteria.

The equations governing the porous cathode model can be solved independently of those governing the separator and the anolyte to obtain the cathodic partial currents, and the required overpotential, given a cell current, catholyte feed composition, temperature and flow rate. For batch simulations, where the concentration of the reactants change with time, the governing equations are integrated into the dynamic equations for the recirculation tanks given previously [8].

3. Experimental details

Before the model could be used to predict the performance of the porous cathode, estimates of the kinetic parameters were needed. The parameters used by Coleman et al. [7] and Prasad et al. [8] were suspect as they were extracted using data which did not measure the flow rate of the product gases and the changes in the catholyte and anolyte volumes with time. Wingard [9] performed parameter estimation using a planar nickel cathode with a more comprehensive set of data. The experimental data, and therefore, the kinetic parameters obtained by Wingard suggested significant differences from the ones used by Coleman et al. [15] and Prasad et al. [16]. To obtain the parameters for porous nickel, batch experiments identical to those done by Wingard [17] were performed, but with a porous rather than a planar cathode.

3.1. *Procedure*

A schematic of the setup used for the experimental batch runs is shown in Figure 2. The divided cell was assembled so that the porous nickel cathode was in the flow-through mode and the planar stainless steel anode was in the flow-by mode. The porous cathode was foam grade with 80 pores per inch and a thickness of 0.30 cm. Prior to turning on the current, a steady-state temperature of 32 °C was obtained. A complete set of physical parameters and operating conditions are shown in Tables 1 and 2. All the experiments ran for 4 h and used a divided MP cell (a multipurpose electrochemical cell developed by Electrocell AB, Sweden) with Nafion® 350 as the cation-selective separator, and 2 M sodium hydroxide (NaOH) solution as the anolyte feed. The

Table 1. Three different catholyte feed concentrations used in the batch runs

Component	Concentration/M		
	Feed 1	Feed 2	Feed 3
$NaNO_3$	0.0	1.95	1.95
$NaNO_2$	0.6	0.0	0.6
NaOH	1.33	1.33	1.33
NaCl	0.281	0.281	0.281
NaBr	0.125	0.125	0.125

Table 2. Physical parameters and operating conditions common to all batch runs. The diffusion coefficient for each species was given elsewhere [8]

Parameter	Value
Current	25 A
Initial anolyte and catholyte volume	3000 cm³
Anolyte and catholyte flow rates	31.5 cm³ s⁻¹
Run time	4 hours
Temperature	32 °C
Cathode porosity, θ	0.87
Interfacial area of cathode, a	60 cm⁻¹
Superficial electrode area, A	100 cm²
Anode and cathode gap, S_a and S_c	0.60 cm
Separator thickness, S_s	0.050 cm
Electro-osmotic drag coefficient, λ_w	10
Conductivity of separator	7.0×10^{-3} Ω^{-1} cm⁻¹
Anode diffusion layer thickness, δ_{OH^-}	19.7×10^{-3} cm

four-hour run was long enough to obtain measurable concentration changes, but short enough that the reaction rates remained constant during the run. The catholyte flow rate listed in Table 2 translates into an average velocity of 5.24 cm s^{-1}. For a reactor length of 10 cm, the corresponding residence time is less than 2 s. The short residence time compared to the long run time validates the assumption of low single-pass conversion (i.e., uniform concentration in the flow direction).

Samples of the off gas, catholyte and anolyte were taken at 30 min intervals from the recirculation tanks. The off gas from the catholyte recirculation tank was passed through a water condenser at 15 °C to minimize the loss of water. Due to the low gas-generation rate, a known flow rate of argon was combined with the off-gas stream. Also at 30 min intervals, the values for the potentials in the three cell compartments (i.e., anode, separator and cathode) with respect to the reference electrodes (Ag/AgCl) were recorded along with the overall cell potential and current. The reference electrode in the cathode section was placed between the separator and the porous cathode, thus minimizing the uncompensated resistance.

The off gas flow rate was measured using a calibrated gas bubble meter and the gas composition was analyzed using a Hewlett–Packard 5890 gas chromatograph (GC). The nitrate and nitrite concentrations in the anolyte and catholyte samples were measured using a Dionex 500 ion chromatograph (IC). The concentration of nitrate and nitrite in the anolyte, and hence their transport across the separator from the catholyte, was found to be negligible. Therefore, the nitrite oxidation reaction (reverse of Equation 1) was negligible and oxygen evolution was the predominant anodic reaction. The hydroxide (OH^{-}) concentration was obtained by titration with glacial acetic acid. The chloride and bromide concentrations, obtained by ion chromatography, were used to determine the dilution of the catholyte from the water moving across the separator. Since the chloride and bromide species do not undergo any reaction and are not transported across the cation selective membrane, their moles in the catholyte should remain equal to the initial moles at all times.

3.2. Partial current calculation

The partial currents for the reactions producing N$_2$, N$_2$O, and H$_2$ (i.e., Reactions 3–5, respectively) were calculated by using their molar gas flow rates (F_i) by:

$$I_k = \frac{n_k \mathscr{F}}{s_{ik}} F_i \tag{16}$$

To obtain the molar flow rates, the volumetric flow rate, Q_g, measured using a bubble flow meter, and the molar composition y_i, measured using the gas chromatograph, were used with the ideal gas law to give

$$F_i = \frac{Q_g y_i P}{\mathscr{R} T} \tag{17}$$

The nitrate to nitrite reduction current was found using the change in moles of nitrate with time as shown below:

$$I_1 = -2\mathscr{F} \frac{dM_{NO_3^-}}{dt} \tag{18}$$

The ammonia production current (Reaction 2) was obtained from a balance on nitrogen containing reactants and products, (i.e., nitrate, nitrite, nitrogen, and nitrous oxide) to give

$$I_2 = 6\mathscr{F} \left(-\frac{dM_{NO_3^-}}{dt} - \frac{dM_{NO_2^-}}{dt} - 2\mathscr{F}_{N_2} - 2\mathscr{F}_{N_2O} \right) \tag{19}$$

In Equations 18 and 19, the time derivatives were obtained by fitting a straight line through the data for the moles of the nitrate and nitrite versus time. A straight line means the reaction rate is constant over the 4 h run. When only nitrite was present in the feed, the time derivative for the nitrate was set to zero.

4. Result and discussion

4.1. Estimation of kinetic parameters

The kinetic parameters needed for the divided cell are the exchange current densities for the cathodic and anodic reactions, and the corresponding transfer coefficients. The parameters for the anodic reaction on stainless steel (i.e., $j_{o,ref,6}$ and α_6) have been determined previously by Wingard [9] from current–voltage experiments. To obtain the kinetic parameters for the cathodic reactions, batch experiments of 4 h duration were used to obtain the cathodic partial currents (I_k), and overpotential (ϕ_c vs reference) for feeds 1 and 2 shown in Table 1. The physical parameters and operating conditions common to all batch runs are shown in Table 2. The resulting values of the kinetic parameters extracted from the model, along with those obtained by Wingard [9] for the anodic reaction, are shown in Table 3.

Table 3. Kinetic parameters of the reactions present in the nitrate and nitrite system

Reaction	Exchange-current densities* $j_{o,ref,k}$/A cm^{-2}	Transfer coefficient α_k
1	1.0×10^{-10}	0.42
2	2.0×10^{-9}	0.49
3	5.0×10^{-15}	0.50
4	1.0×10^{-15}	0.50
5	1.0×10^{-5}	0.50
6	2.25×10^{-4}	0.81

*Exchange current densities and transfer coefficients for Reactions 1–5 were extracted using experimental data and model. Values for Reaction 6 were obtained previously [9]. Reference conditions are feed 3 concentrations at 32 °C.
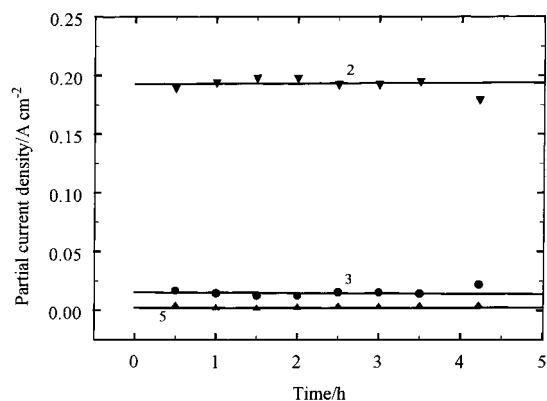
Fig. 4. Partial currents for cathodic reactions at a porous electrode for model simulations (solid lines) and experimental data (symbols). Initial catholyte was feed 1 given in Table 1, and remaining physical parameters and operating conditions are given in Tables 2 and 3. Numbers on the figure correspond to reaction numbers.

Fig. 6. Moles of nitrite and hydroxide in catholyte, and the overpotential at porous cathode, for model simulations (solid lines) and experimental data (symbols). Initial catholyte was feed 1 given in Table 1, and remaining physical parameters and operating conditions are given in Tables 2 and 3.

The experimental (symbols) and simulated (solid lines) partial currents are shown in Figures 4 and 5 for feeds 1 and 2, respectively. The model predictions show good agreement with the experimental results. These results show that Reaction 2 (ammonia production) is the dominant reaction in the case of both nitrite and nitrate feeds (i.e., feeds 1 and 2). Reaction 1 (i.e., nitrate to nitrite reduction) was the second largest reaction when nitrate was present in the feed (i.e., feed 2).

The experimental and simulated values for the moles of nitrate, nitrite, and hydroxide, and the cathodic overpotential are shown in Figures 6 and 7 for feeds 1 and 2, respectively. Again, the model predictions for the moles and overpotential show good agreement with the experimental results. The linear change in the moles of nitrate and nitrite in the Figures justifies the use of a straight line fit for partial current calculations as discussed earlier (see Equations 18 and 19). The moles of hydroxide are an independent check of the model since hydroxide moles were not used in the parameter estimation.
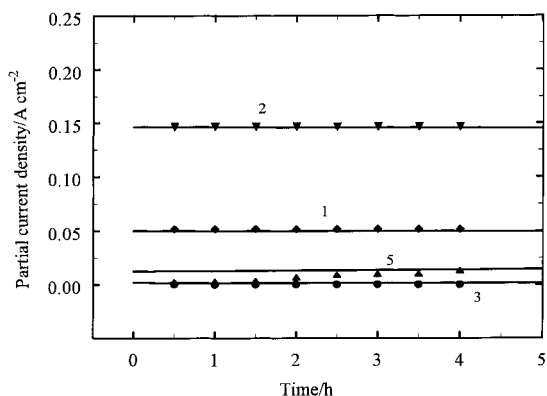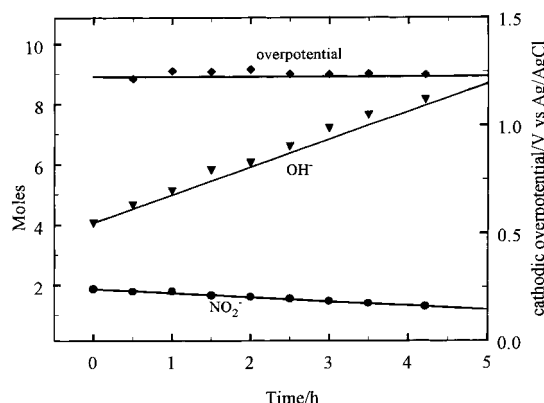
4.2. Comparison of planar and porous cathodes

Using the kinetic parameters extracted from the experimental data, dynamic simulations for feed 3 are shown in Figures 8–10 for a cell with a planar (dashed line) and a porous (solid line) cathode. This feed concentration corresponds to the nitrate, nitrite and hydroxide concentrations in the low-level waste stream shown in Figure 1. Figure 8 shows the change in the moles of nitrate and nitrite with time. For illustrative purposes, the times after which 95% of the initial moles of the nitrate and nitrite were destroyed are also shown in Figure 8. In the porous cathode, the moles of nitrate and nitrite change linear with time throughout the batch run. The slope of this line, however, changes abruptly after 15 h, once the nitrite is depleted. The linearity of the moles versus time results from the near 100% current efficiency that occurs in the porous cathode. In contrast, the nonlinear decay of nitrate and nitrite on the planar cathode is indicative of the significant hydrogen evolution that continues to increase throughout the run.

Fig. 5. Partial currents for cathodic reactions at a porous electrode for model simulations (solid lines) and experimental data (symbols). Initial catholyte was feed 2 given in Table 1, and remaining physical parameters and operating conditions are given in Tables 2 and 3. Numbers on the figure correspond to the reaction numbers.
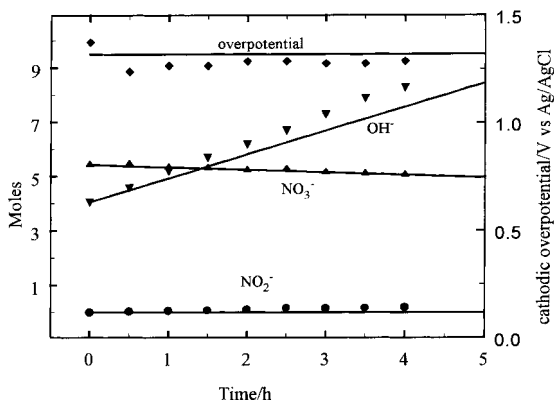

Fig. 7. Moles of nitrate, nitrite and hydroxide in catholyte, and overpotential at the porous cathode, for model simulations (solid lines) and experimental data (symbols). Initial catholyte was feed 2 given in Table 1, and remaining physical parameters and operating conditions are given in Tables 2 and 3.
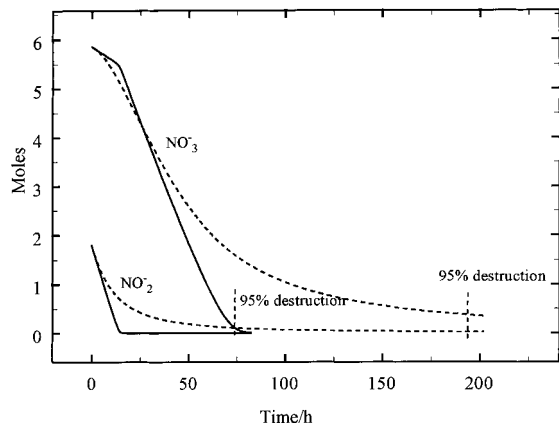
Fig. 8. Moles of nitrate and nitrite in the catholyte containing a porous (solid lines) and planar (dashed lines) cathode. Initial catholyte was feed 3 given in Table 1, and remaining physical parameters and operating conditions are given in Tables 2 and 3. The 95% destruction points are also indicated for both porous (70 h) and planar (195 h) cathodes.

The overall efficiency of the process can be accessed by evaluating the time needed to destroy 95% of the initial moles. From Faraday's law, the time required to reduce 3 liters of 1.95 M $NaNO_3$ and 0.6 M $NaNO_2$, with ammonia being the only product (i.e., 100% efficiency based on all nitrate and nitrite reduction resulting in ammonia as the final product), is about 62 h for a cell current of 25 A. The porous cathode used 75 h as seen from Figure 8. Therefore, the process operated at an overall efficiency of more than 80% based on ammonia. The planar cathode however, used approximately 200 h and therefore, operated at only 30% efficiency. The time for 95% destruction of nitrate and nitrites using a porous cathode is approximately one third of that using a planar one. Therefore, there is definite advantage in using a porous cathode from the standpoint of destruction time (i.e., coulombs passed).

To gain further insight into the reduction process, the partial current fractions for the porous and planar

cathodes are shown in Figure 9 as a function of time. For example, this current breakdown reveals why a discontinuity in the slope is seen in Figure 8 for the porous cathode. Nitrite to ammonia (Reaction 2) consumes most of the current during the first 15 h of operation. Once the nitrite is gone, nitrate to ammonia (Reaction 1 plus 2) dominates, thus dramatically increasing the rate of nitrate destruction. The net effect is that ammonia production dominates throughout most of the run for the porous cathode. In contrast, ammonia production dominates for approximately 25% of the run on the planar cathode. During the final 100 hours, most of the current is going into hydrogen evolution (Reaction 5). The hydrogen evolution reaction becomes significant earlier for the planar cathode compared to the porous cathode due to its lower surface area, and hence higher overpotentials. In the porous cathode, the hydrogen reaction current only increases rapidly when more than 95% of the nitrates and nitrites are reduced. This means that destroying more than 95% of the waste will significantly increase operating costs. Capital costs will also rise since more electrolysers will be needed to treat a fixed amount of waste in a given time.

The simulation results for the voltages in the electrochemical cell are shown in Figure 10 for porous (solid lines) and planar (dashed lines) cathodes. The ohmic drop is the major component of the cell voltage and it changes with time due to changes in the conductivity of the catholyte. The conductivity of the catholyte increases initially due to production of more hydroxide ions. However, it starts to decrease later due to gradual depletion of nitrate and nitrite ions. The cathodic overpotential increases with time for both the porous and planar electrodes due to depletion of nitrate and nitrite ions. A sharp increase in the cathodic overpotential is seen for the porous cathode when the nitrite in the solution is depleted after about 15 h. The cathodic overpotential for the porous cathode is always lower than the planar electrode due to higher surface areas,
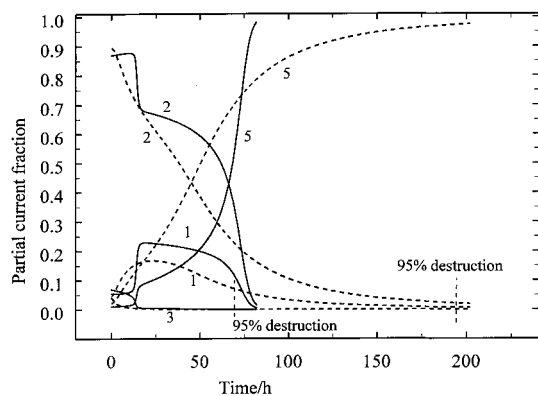

Fig. 9. Partial currents for cathodic reactions at a porous (solid lines) and planar (dashed lines) cathode. Initial catholyte was feed 3 given in Table 1, and remaining physical parameters and operating conditions are given in Tables 2 and 3. Numbers on the Figure correspond to reaction numbers. The 95% destruction points are also indicated for both the porous (70 h) and planar (195 h) cathodes.
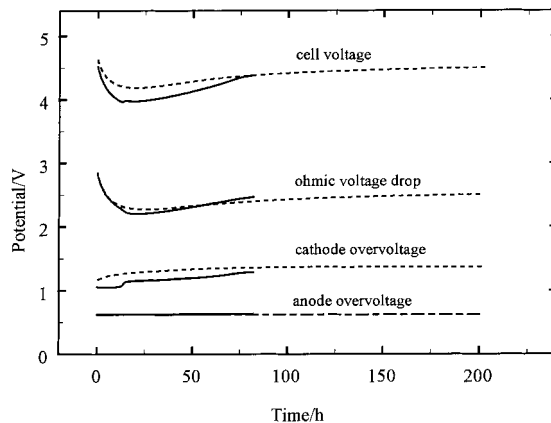

Fig. 10. Potentials at a porous (solid lines) and planar (dashed lines) cathode. Initial catholyte was feed 3 given in Table 1, and remaining physical parameters and operating conditions are given in Tables 2 and 3. The 95% destruction points are also indicated for both the porous (70 h) and planar (195 h) cathodes.

and hence lower reaction current densities. Although the cathodic overpotentials do not appear very different between the two electrodes, the 100–200 mV difference is enough to effect the hydrogen evolution rate. The anodic overpotential stays constant at approximately 0.6 V due to constant replenishment of the anolyte.

To illustrate the destruction efficiency of porous cathodes of different thicknesses and that of a planar cathode, the destruction current density (sum of current densities of Reactions 1–4) is plotted versus the cell current density in Figure 11. The results are shown for concentrations corresponding to feed 3 in Table 1 (solid lines) and concentrations of nitrate and nitrite after 95% destruction (dashed lines). For the purposes of illustration, a nitrate concentration 0.13 M and a nitrite concentration of 0.0 M was chosen as the value corresponding to the 95% destruction point. At feed 3 concentrations, the destruction current rises linearly with the cell current for both planar and porous cathodes for current densities lower than 0.3 A cm^{-2}, indicating 100% destruction efficiency (i.e., negligible hydrogen evolution). As the destruction current becomes mass-transfer limited, the slope of the curve approaches zero and hydrogen evolution begins to dominate. At very high cell currents, the destruction current starts to decrease due to the repulsion of the negative ions from the cathode.

A peak in the destruction currents is seen in Figure 11 for the planar electrode, and the porous electrode with a thickness of 0.05 cm. Peaks are not shown for the other porous cathodes. Instead, the simulations were stopped when the onset of mass transfer limitation was observed. The cell current at which the peak in the destruction current occurs is lowest for a planar cathode. The peak in the destruction current for a planar cathode is approximately one-half that for a porous cathode of thickness of 0.05 cm. As expected, the plots obtained at concentrations corresponding to 95% destruction show that the inefficiencies become larger for both electrodes due to lower reactant concentrations. The planar cathode operates at an efficiency less than 50% for a cell current greater than 0.1 A cm^{-2}. The large change in the efficiency with concentration for a planar cathode suggests that an optimization of the operating current with percent destruction is required. Such a scenario was examined by Prasad et al. [8]. However, the optimization is probably not necessary in a thick porous cathode due to relatively high efficiencies even at concentrations after 95% destruction of nitrates and nitrites.

Increasing the thickness of a porous cathode at feed 3 concentrations from 0.05 cm to 0.3 cm increases the peak destruction current and the corresponding cell current due to a delay in the onset of mass-transfer limitations. The higher reaction area per cross-sectional area offered by a thicker cathode has limits as an increase in the cell current results in a more nonuniform reaction distribution. Therefore, a cell current is reached that results in very little reaction deep inside the pores due to ohmic resistance. Increasing the thickness of the electrode beyond 0.3 cm increases the cost of the electrode without providing additional useable surface area.

The increase in the nonuniformity of the reaction currents with an increase in the cathode thickness is illustrated in Figure 12. The figure shows the profile of the normalized reaction currents versus the normalized bed depth for the cell current density used in the experiments (i.e., 0.25 A cm^{-2}) and for electrode thicknesses of 0.05 (dashed line) and 0.5 cm (solid line). The reaction currents are normalized using the average reaction current (i.e., I_{cell}/aAL) while the bed depth is normalized using the electrode thickness, L. The reactions are highest in the front of the electrode due to higher overpotentials. For the thinner electrode, the ohmic drop inside the electrode is lower, the reaction is more uniform throughout, and the electrode is fully
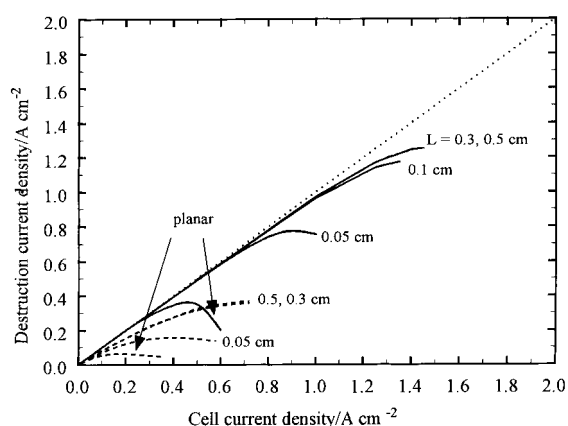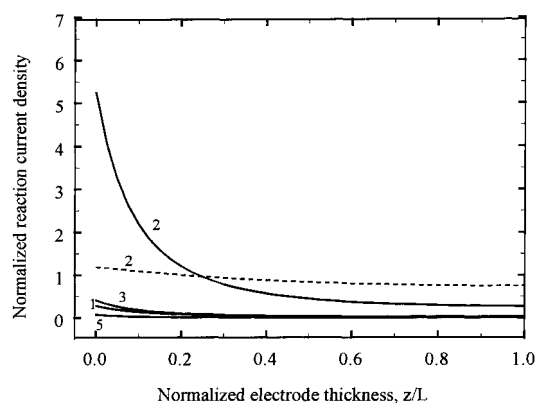

Fig. 11. Effect of cell current on destruction current for porous and planar electrodes. Destruction current is defined as the sum of the currents from Reactions 1–4. Catholyte was feed 3 given in Table 1 (solid lines) and concentration after 95% destruction (dashed lines). Remaining physical parameters and operating conditions are given in Tables 2 and 3.

Fig. 12. Normalized reaction distribution in a porous electrode of thickness 0.30 cm (solid lines) and 0.05 cm (dashed lines). Numbers on figure correspond to Reaction numbers. Reaction 2 is the only significant reaction occurring in the thin electrode. Catholyte was feed 3 given in Table 1, and remaining physical parameters and operating conditions are given in Tables 2 and 3.

utilized. In contrast, very little reaction occurs towards the back of the thicker electrode. Therefore, increasing the electrode thickness beyond 0.5 cm will have very little effect on the behaviour of the electrode. The reaction nonuniformity is enhanced at higher currents, resulting in the indistinguishable difference between the 0.3 and 0.5 cm thick electrode in Figure 11.

Efficiency effects seen in Figure 11, though, are not enough to determine optimum cell design and operation. Other performance criteria will result in different optimum conditions. Therefore, two additional performance criteria are evaluated for destroying 95% of the nitrates and nitrites in feed 3: (i) time and (ii) total energy. Process time and energy consumption are directly related to the capital costs and operating costs, respectively. Equating process time to capital costs assumes that a fixed amount of waste must be processed over a fixed period of time (e.g., 20 million gallons over 20 years). For example, halving the batch time means doubling the number of electrolyzers required to treat the waste. The basis for the following analysis will be a one-liter batch with cathodes having a superficial area 100 cm^2.

Figure 13 shows the process time versus current density for porous (solid line) and planar (dashed line) electrodes. At the porous electrode, the process time decreases with current. This is consistent with Figure 11, which shows that for these electrode thicknesses the destruction current increases with increasing current between 0 and 0.75 A cm^{-2}. At the planar electrode, a minimum of approximately 55 h of processing time is observed at 0.2 A cm^{-2}. Increasing the current beyond 0.2 A cm^{-2} increases the processing time because at high currents the destruction current actually decreases with increasing current (see Figure 11). However, even the minimum time required by the planar electrode is more than double that required by the porous cathode for the same current. At 0.40 A cm^{-2}, the time needed to process the waste is an order-of-magnitude lower for the porous electrode compared to that of the planar.
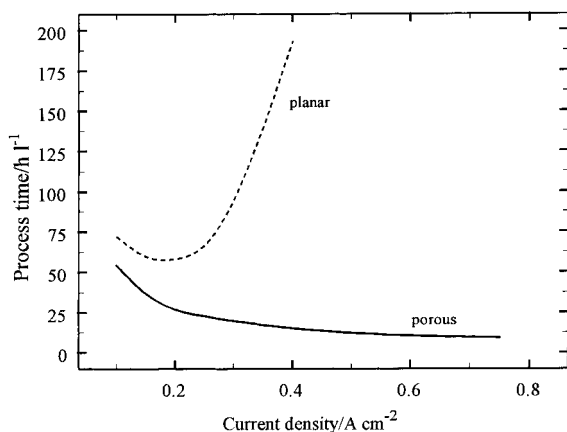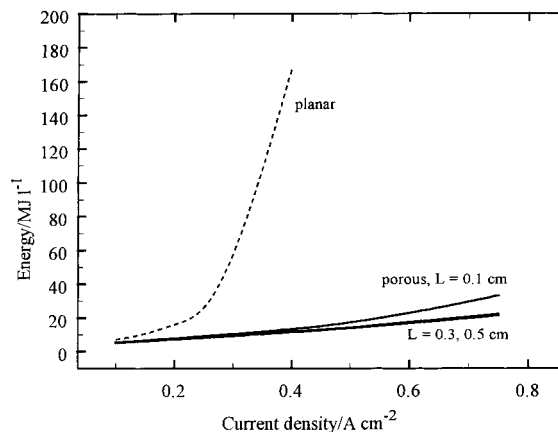

Fig. 14. Effect of cell current on the energy needed to destroy 95% of nitrate and nitrite in feed 3 at a porous (solid lines) and planar (dashed lines) cathode. Physical parameters and operating conditions are given in Tables 2 and 3.

Figure 14 shows the energy costs versus current for the porous and planar electrodes. At the lowest current density (i.e., 0.1 A cm^{-2}) the energy used in the porous and planar electrodes is similar. However, increasing the cell current increases the energy much more rapidly in the planar compared to the porous cathodes. This is due to the increase in destruction time and larger cell voltage needed for the planar cathode. Increasing the cell current beyond 0.25 A cm^{-2} results in an exponential increase in the energy required. The exponential increase in energy is due to the increase in the destruction time seen in Figure 13. The energy used for the porous cathode increases approximately linearly with cell current due to ohmic control of the cell voltage (see Figure 10). Thicker electrodes use less energy than thinner one, especially at high currents. However, mechanical integrity and electrode cost will probably dictate electrode thickness rather than energy usage.

5. Conclusions

Experimental batch cell data was collected to determine the kinetic parameters for nitrate and nitrite reduction at 32 °C. This was used in conjuction with a mathematical to compare the performance of porous and planar cathodes. Comparisons between these two electrodes indicate definite advantages in using porous cathodes for nitrate and nitrite destruction. For example, at a cell current of 0.25 A cm^{-2}, the porous cathode needed one-third the time and energy required to destroy 95% of the nitrates and nitrites compared to the planar cathode. At 0.40 A cm^{-2}, the porous cathode needed an order-of-magnitude less time and energy. The thickness of the porous electrode is relatively unimportant from a processing standpoint. The choice of electrode thickness will probably be determine based on mechanical integrity and electrode cost. The final selection of a porous or a planar cathode, however, will depend on the relative cost of electricity and capital,

Fig. 13. Effect of cell current on the time needed to destroy 95% of nitrate and nitrite in feed 3 at a porous (solid lines) and planar (dashed lines) cathode. Porous cathode was 0.30 cm thick, and other physical parameters and operating conditions are given in Tables 2 and 3.

and on the required destruction criteria. For example, if electricity costs are the major consideration, then low currents are desirable, thus reducing the advantage of the porous electrode. In contrast, high capital costs would favour high currents, and consequently they would favour the use of porous cathodes. Lowering the destruction criteria from 95% to 80% would also improve the performance of the planar cathode relative to the porous. A higher percent destruction would further favour the porous electrode. The percent destruction would depend on the cost of depositing the low-level saltstone compared to the cost of electrochemically destroying the nitrates and nitrites.

Acknowledgements

Appendix

Derivation of Equation 17

When there is no slip between the gas and liquid phase, the gas void fraction in a porous electrode is related to the volumetric flow rates of the gas and liquid phases, and the porosity of the electrode, by

$$\theta_g = \theta \frac{Q_g}{Q_l + Q_g} \tag{20}$$

Using the chain rule, the gradient in the gas porosity can be written as

$$\frac{d\theta_g}{dz} = \theta \frac{(Q_l + Q_g)\frac{dQ_g}{dz} - Q_g\frac{dQ_g}{dz} - Q_g\frac{dQ_l}{dz}}{(Q_l + Q_g)^2} \tag{21}$$

For porous electrodes with low per-pass conversion, the change in the volumetric flow of the liquid, Q_l, is negligible with electrode depth, z, and therefore its gradient can be neglected in the above equation. This assumption can be used to simplify the above equation to

$$\frac{d\theta_g}{dz} = \theta \frac{Q_l \frac{dQ_g}{dz}}{(Q_l + Q_g)^2} \tag{22}$$

Equation 20 can be written as follows after re-arranging the terms and recognizing that $Q_l/Q_g = (\theta - \theta_g)/\theta_g$:

$$(Q_l + Q_g)^2 = Q_l^2 \frac{\theta^2}{(\theta - \theta_g)^2} \tag{23}$$

Substituting equation 23 in equation 22 results in the following equation:

$$\frac{d\theta_g}{dz} = \frac{(\theta - \theta_g)^2}{\theta Q_l} \frac{dQ_g}{dz} \tag{24}$$

Using Faraday's law and the ideal gas, the change in the volumetric flow rate of the gas can be related to the sum of the local rates of the gas producing reactions as follows:

$$\frac{dQ_g}{dz} = a \frac{\mathscr{R}TA}{P\mathscr{F}} \sum_{k=2}^{5} \frac{j_k}{n_k} \tag{25}$$

Substituting Equation 25 in Equation 24, the gradient in the gas porosity can be expressed as follows:

$$\frac{d\theta_g}{dz} = a \left(\frac{\mathscr{R}TA(\theta - \theta_g)^2}{P\mathscr{F}\theta Q_l} \right) \sum_{k=2}^{5} \frac{j_k}{n_k} \tag{26}$$

References

1. D.T. Hobbs and M. Ebra, *AIChE Symp. Series No.254* **83** (1987) 149.
2. D.T. Hobbs, G.D. Genders and D. Hartsough, Abstract 568, The Electrochemical Society Extended Abstracts, Vol. **94-1**, San Francisco, CA, 22–27 May (1994), p. 910.
3. Hu-lin Li, D. Robertson, J. Chambers and D.T. Hobbs, *J. Electrochem. Soc.* **135**, (1988) 1154.
4. D.T. Hobbs, 'Electrochemical treatment of nuclear waste at Savannah River Site' in J.D. Genders and N. Weinberg (eds) 'Electrochemistry for a Cleaner Environment', (The Electrosynthesis Company, Amherst, New York, 1992).
5. J.O'M. Bockris and J. Kim, *J. Electrochem. Soc.* **143**, (1996) 3801.
6. J.O'M. Bockris and J. Kim, *J. Appl. Electrochem.* **27**, (1997) 623.
7. D. Coleman, R.E. White and D.T. Hobbs, *J. Electrochem. Soc.* **142**, (1995) 1152.
8. S. Prasad, J. Weidner and A. Farell, *J. Eectrochem. Soc.* **142**, (1995) 3815.
9. D. Wingard, 'An Analysis of the Batch Electrochemical Reduction of NO_3^-/NO_2^- in Low-Level Radioactive Waste', PhD dissertation (University of South Carolina, Columbia, SC, 1995).
10. M. Saleh, J. Weidner, B. El-Anadouli and B. Ateya, *J. Electrochem Soc.* **142**, (1995) 4122.
11. J. Newman, 'Electrochemical Systems', 2nd edn. (Prentice Hall, Englewood Cliffs, NJ, 1991).
12. S. Langlois and F. Coeuret, *J. Appl. Electrochem.* **19**, (1989) 51.
13. D. Bruggeman, *Ann. Physik.* **24**, (1935) 636.
14. E. Kreyszig, 'Advanced Engineering Mathematics', 5th edn. (Wiley Eastern Ltd, 1983).